

Edge and core confinement in improved H-modes in ASDEX Upgrade

C.F. Maggi, R. Bilato, M. Brambilla, J.C. Fuchs, B. Kurzan, L.D. Horton, Y.-S. Na¹,
E. Poli, A.C.C. Sips, A. Stabler, J. Stober, W. Suttrop, G. Tardini, E. Wolfrum
and the ASDEX Upgrade Team

MPI fur Plasmaphysik, EURATOM Association, D-85748 Garching, Germany

¹*Korea Basic Science Institute, 52 Yeoeun-Dong, Yusung-Gu, Dejeon, 305-333, Korea*

1. Improved H-modes in ASDEX Upgrade

The improved H-mode is an interesting scenario for ITER, since it combines high confinement ($H_{98}(y,2) > 1$) with high stability ($\beta_N > 2.5$) in stationary discharges (longer than $40 \times \tau_E$ or more than twice the current diffusion time) and the absence of sawteeth activity [1]. Typically, improved H-modes are operated at low ν^* and with $T_i > T_e$.

Whereas T_i profiles are stiff in improved H-modes with the same gradient length as in standard H-modes [2], one aspect of the confinement improvement with respect to the reference ELMy H-mode scenario is density peaking: higher core densities lead to higher stored energies, at fixed temperature profiles. Performance improvement due to density peaking is limited by impurity accumulation and the concomitant increase in core radiation [3]. Control of density peaking (and impurity accumulation) has been established as a routine tool in ASDEX Upgrade (AUG) using central wave heating (both ICRH and ECRH) [3]. Improved H-modes have also been obtained with strong central ICRH (up to half of the total input power) with the goal of exploring heating conditions similar to those of a reactor.

The other aspect of confinement improvement is the role of the edge transport barrier (ETB). There are indications that the contribution to the global confinement from the ETB region increases with input power. To test this hypothesis detailed measurements of the pedestal parameters were carried out recently in AUG in discharges where the confinement is improved with increasing input power.

2. Confinement improvement and density peaking

In Fig. 1 the confinement factor $H_{98}(y,2)$ is plotted versus the density peaking factor, defined as $n_e(\rho_{pol} = 0.1)/n_e(\rho_{pol} = 0.9)$. The electron density profile was obtained by fitting simultaneously the data from the core Thomson scattering (TS) diagnostic, the five horizontal interferometer channels and the edge Li-beam data when available. The electron temperature profile was obtained by fitting simultaneously the data from the core TS diagnostic and from the ECE diagnostic. In the absence of edge measurements the pedestal region was fitted assuming a fixed position for the pedestal top and a constant pedestal width of $\Delta\rho_{pol} = 0.02$ for both electron density and temperature profiles.

Although there are some doubts concerning the validity of the ITER-98(y,2) H-mode scaling at high values of β_N and with respect to density dependence, in Fig.1 a large number of discharges can be compared over a wide parameter range. It is found that high density peaking factors are correlated with the highest values of $H_{98}(y,2)$, but that there is a large excursion in confinement factor, for a given value of density peaking, in the range between 1.0 and 2.0. Analysis of selected discharges (open circles in Fig. 1), lying at the extreme ends of $H_{98}(y,2)$ variation at fixed density peaking, shows that the confinement improves with increasing electron pressure at the top of the pedestal, p_e^{PED} . The arrows join phases where the input power is increased (red to green circle) within the same discharge. This leads to an increase of total stored energy due to an increase of electron pedestal pressure, while: i) the density peaking remains constant, or ii) the density peaking increases, or iii) the density peaking decreases.

In Fig. 2 the density peaking factor is plotted versus the effective collisionality ν_{eff} at mid radius, defined as in [4], where a constant value of $Z_{\text{eff}} = 2$ is assumed. For NB heated discharges the general trend of higher density peaking at low ν_{eff} is found. The scatter in the data is larger compared to [4], where only H-modes with 5 MW NB heating were considered. With ICRH, flattening of the density profile at low ν_{eff} is observed. In this regime TEM's are the dominant instability and density flattening is expected when central electron heating is applied [5].

3. Confinement improvement and role of the pedestal region

New detailed measurements of the pedestal profiles were carried out in recent improved H-modes, where the input power was increased with three NB power steps up to 10 MW. A constant level of central ICRH heating was added in order to avoid strong density peaking, with 3 MW of power coupled to the plasma. The pedestal parameters, including the value at the pedestal top and the pedestal width Δ , were obtained from fits to the ECE and edge TS data for T_e , to the Li-beam and edge TS data for n_e and to the core CXRS data for T_i , assuming fixed pedestal T_i position and $\Delta_{T_i} = 0.02$. A dilution factor $f_{\text{DIL}} = n_i/n_e = 0.8$ is used for the estimate of the ion density n_i . Using this value as input to the NB Monte Carlo code FAFNER [6] results in calculations of the total stored energy W_{tot} that are consistent with magnetic measurements (W_{mhd}) within 10% or better. The measured neutron rate, however, is overestimated by a factor of two. Power deposition profiles from ICRH to plasma ions and electrons are calculated with the TORIC code for wave propagation and absorption [7] and a quasi-linear Fokker Planck solver for fast ions coupling to the bulk plasma [8]. Because of the high concentration of H minority ($\sim 17\%$) and low RF power (3 MW) in these discharges, the fast ion contribution from ICRH to the total stored energy is negligible and this heating scheme heats predominantly the plasma ions.

During the power ramp the density peaking factor remains constant at a value of ~ 1.4 . The variation of W_{th} and W_{PED} with total input power is plotted in Fig. 3. A dependence of $W_{\text{PED}} \sim P_{\text{TOT}}^{0.59}$ and $W_{\text{th}} \sim P_{\text{TOT}}^{0.69}$ is found. By overlaying the results of these experiments (red squares) with the scaling for the electron pressure at the top of the pedestal for AUG type I ELMy H-modes found using the database described in [9] (Fig. 4), a stronger dependence on input power is found for the improved H-mode discharge of Fig. 3 than that of the broad database, for which the electron pedestal pressure scales as $P_{\text{TOT}}^{0.2}$. Note that the data for the type I ELMy H-mode database are taken from the TS diagnostic at fixed $\rho_{\text{pol}} = 0.9$, whereas the data from this analysis are actual fits of the measured pedestal region. The blue triangles in Fig. 4 represent the electron pressure for the improved H-mode discharge calculated from the fitted profiles at $\rho_{\text{pol}} = 0.9$ and give a power dependence of $p_e(\rho_{\text{pol}} = 0.9) \sim P_{\text{TOT}}^{0.93}$, showing that the offset between pedestal top and $\rho = 0.9$ surface is important. However, even at the pedestal top, a significant input power dependence, $p_e(\text{PED-top}) \sim P_{\text{TOT}}^{0.61}$, is found for this discharge.

The observed increase of pedestal pressure with input power occurs for different reasons at each power step. In the first step, from 7.6 to 9.6 MW, the increase in pedestal pressure is due to an increase in density, while T_e and T_i both decrease slightly. This density increase is, in turn, due to an increase in the separatrix density. Therefore, in this first power step the increase in pedestal pressure, and the consequent global confinement increase, is found to be largely a SOL effect. In the second power step, from 9.6 to 11.3 MW, the pedestal pressure increases largely due to increases in the electron and ion temperature. The increased pedestal electron temperature is due to an increased slope rather than an increase of the pedestal width. Ideal MHD calculations of the stability limit in these discharges are planned for the near future.

4. Effect of central heating with ICRH and ECRH

An additional aim of this experiment was to try to quantify the relative magnitude of central ion and electron heating and its effect on density peaking. Therefore, in a discharge similar to that described above, the ICRH heating was switched off during the NBI power ramp and 1.2 MW of ECRH heating were added in the second phase of the pulse. Calculations of the ECRH power deposition profile carried out with the TORBEAM code [10] show a narrow power deposition profile at $\rho_{\text{pol}} = 0.37$ ($\rho_{\text{tor}} = 0.25$).

ASTRA [11] calculations of ion and electron heat fluxes (q_i and q_e) show that in the NBI+ICRH cases (independently of the total input power) $q_i/q_e > 1$ over the whole plasma radius, whereas for the NBI+ECRH cases q_i/q_e is changed significantly inside the confinement region, with q_e approaching q_i . This is illustrated in Fig. 5 for the time slices corresponding to the second NB power step. However, the total amount of central heating (electron+ion), e.g. inside $\rho_{\text{tor}} \sim 0.3$, is essentially unchanged with the two heating schemes for the given injected powers. Since the density peaking factor does not vary during the discharge, this result may suggest that it is the total amount of central heating to be responsible for the flattening of the density profile, rather than the contribution from the electron channel alone. In a third discharge, the ICRH heating was switched off during the second NB power step and then the pulse was run with the NBI power ramp only. The density profile became very peaked and the discharge became unstable due to impurity accumulation. Switching off the ICRH heating corresponds - at $\rho_{\text{tor}} = 0.3$ in Fig. 5 - to removing 0.5 MW from the electron heat flux and 1.5 MW from the ion heat flux.

5. First comparisons with predictive transport analysis

In order to understand the transport in the core region, simulations of the discharges discussed in Sect. 3 and 4 were carried out with ASTRA in a predictive mode using the GLF23 transport model [12]. The boundary condition was fixed at $\rho_{\text{tor}} = 0.8$. The model reproduces fairly well the measured T_e , n_e and T_i profiles across the confinement region, $\rho_{\text{tor}} \sim 0.3 - 0.8$. The one exception is that the simulations predict a higher T_i gradient in the confinement region in the lower power phase. In the plasma center ($\rho_{\text{tor}} < 0.3$) the model overpredicts the experimental profiles. In this region the code predicts the transport to be predominantly neoclassical. A possible explanation for this difference could be MHD activity in the plasma core (e.g. fishbones), which may introduce additional transport not accounted for in the model. In any case, the global confinement is relatively insensitive to this core region due to its small volume.

References:

- [1] A. Stabler et al., to appear in Nucl. Fusion.
- [2] Y-S. Na et al., Plasma Phys. Control Fusion **44** (2002) 1285.
- [3] R. Neu et al., Nucl. Fusion **45** (2005) 209.
- [4] C. Angioni et al., Phys. Rev. Lett. **90** (2003) 205003.
- [5] C. Angioni et al., Nucl. Fusion **44** (2004) 827.
- [6] G.G. Lister, IPP Report 4/222 (1985).
- [7] M. Brambilla et al., Plasma Phys. Control. Fusion **41** (1999) 1-34.
- [8] M. Brambilla et al., Nucl. Fusion **34** (1994) 1121-43.
- [9] H. Urano et al., Plasma Phys. Control. Fusion **45** (2003) 1571.
- [10] E. Poli et al., Comp. Phys. Comm. **136** (2001) 90.
- [11] G. Pereverzev, P.N. Yushmanov, IPP 5/98 (2002).
- [12] R.E. Waltz et al., Physics of Plasmas **4** (1997) 2482.

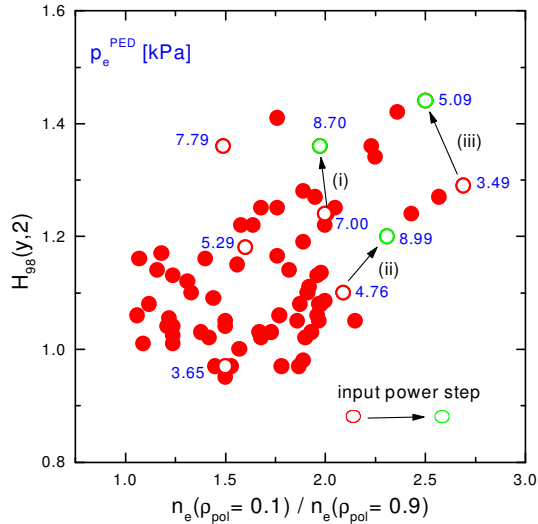


Figure 1. $H_{98}(y,2)$ versus density peaking factor for improved H-modes in AUG.

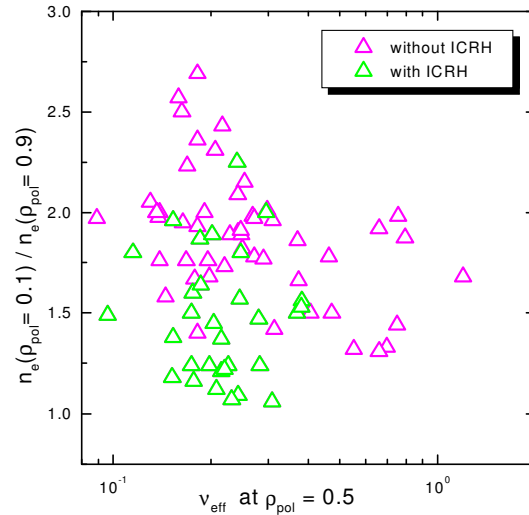


Figure 2. Density peaking factor vs v_{eff} for AUG improved H-modes.

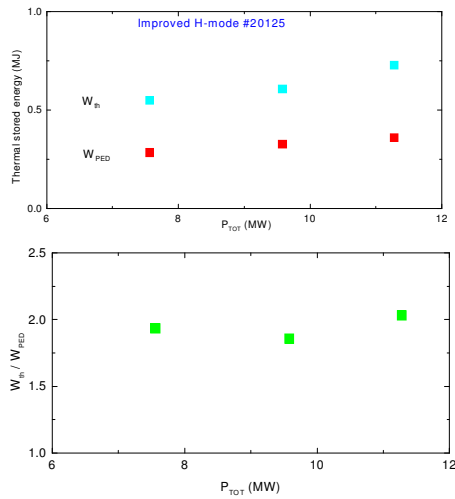


Figure 3. W_{th} and W_{PED} vs total input power for the three power steps of #20125.

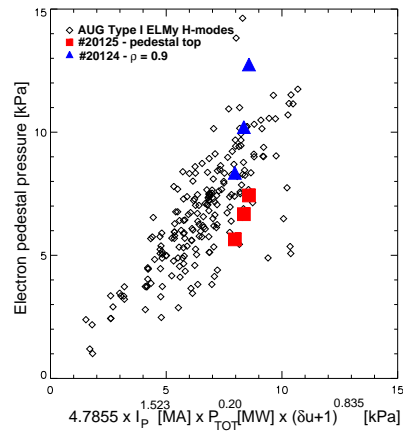


Figure 4. Electron pedestal pressure vs scaling.

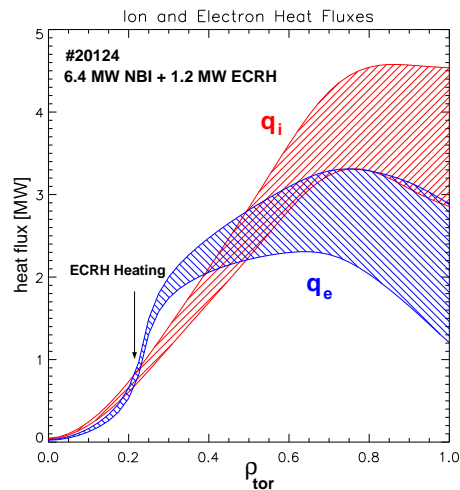
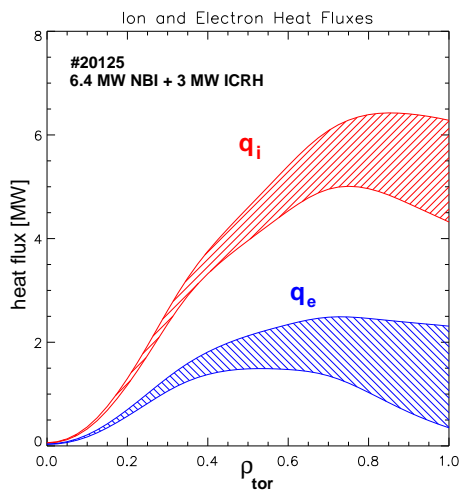


Figure 5. Electron and ion heat fluxes from ASTRA for two similar improved H-mode discharges, one with NBI + ICRH heating and the other with the ICRH replaced by ECRH.